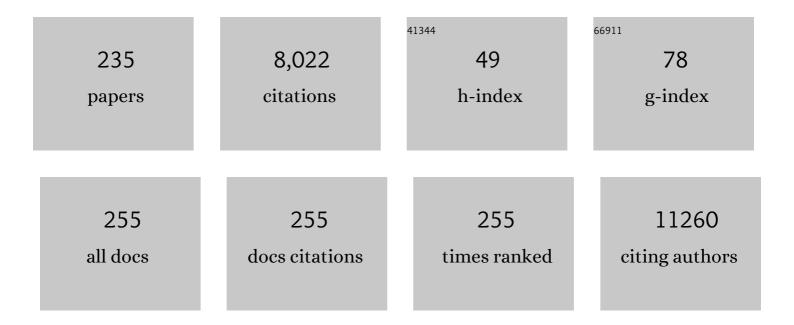
## Keon-Wook Kang

List of Publications by Year in descending order

Source: https://exaly.com/author-pdf/8436883/publications.pdf

Version: 2024-02-01



#	Article	IF	CITATIONS
1	Phase 1 Study of No-Carrier Added 177Lu-DOTATATE (SNU-KB-01) in Patients with Somatostatin Receptor–Positive Neuroendocrine Tumors: The First Clinical Trial of Peptide Receptor Radionuclide Therapy in Korea. Cancer Research and Treatment, 2023, 55, 334-343.	3.0	2
2	A Negative Correlation Between Blood Glucose Level and 68ÂGa-DOTA-TOC Uptake in the Pancreas Uncinate Process. Nuclear Medicine and Molecular Imaging, 2022, 56, 52-58.	1.0	3
3	Identification of alternative protein targets of glutamate-ureido-lysine associated with PSMA tracer uptake in prostate cancer cells. Proceedings of the National Academy of Sciences of the United States of America, 2022, 119, .	7.1	13
4	Comparison of voxel <i>S</i> â€value methods for personalized voxelâ€based dosimetry of <sup>177</sup> Luâ€DOTATATE. Medical Physics, 2022, 49, 1888-1901.	3.0	7
5	Visualization of a novel human monoclonal antibody against Claudin-3 for targeting ovarian cancer. Nuclear Medicine and Biology, 2022, 114-115, 135-142.	0.6	Ο
6	The Impact of the Amendment of the Health Insurance Coverage for F-18 Fluorodeoxyglucose Positron Emission Tomography on the Healthcare Behaviors for Breast Cancer: An Interrupted Time Series Analysis of the Korean National Data From 2013 to 2018. Journal of Korean Medical Science, 2022, 37, e153.	2.5	0
7	AC and DC magnetic softness enhanced dual-doped γ-Fe2O3 nanoparticles for highly efficient cancer theranostics. Applied Materials Today, 2022, 28, 101533.	4.3	4
8	Visual interpretation of [18F]Florbetaben PET supported by deep learning–based estimation of amyloid burden. European Journal of Nuclear Medicine and Molecular Imaging, 2021, 48, 1116-1123.	6.4	17
9	Functional Imaging and Peptide Receptor Radionuclide Therapy for Pancreatic Neuroendocrine Tumor. The Korean Journal of Pancreas and Biliary Tract, 2021, 26, 10-14.	0.1	2
10	Imaging in Tumor Immunology. Nuclear Medicine and Molecular Imaging, 2021, 55, 225-236.	1.0	2
11	Efficacy of voxel-based dosimetry map for predicting response to trans-arterial radioembolization therapy for hepatocellular carcinoma. Nuclear Medicine Communications, 2021, Publish Ahead of Print, 1396-1403.	1.1	0
12	Glucose metabolic profiles evaluated by PET associated with molecular characteristic landscape of gastric cancer. Gastric Cancer, 2021, , 1.	5.3	2
13	International consensus on the use of [18F]-FDG PET/CT in pediatric patients affected by epilepsy. European Journal of Nuclear Medicine and Molecular Imaging, 2021, 48, 3827-3834.	6.4	13
14	Effect of TSH stimulation protocols on adequacy of low-iodine diet for radioiodine administration. PLoS ONE, 2021, 16, e0256727.	2.5	2
15	Fully automated identification of brain abnormality from whole-body FDG-PET imaging using deep learning-based brain extraction and statistical parametric mapping. EJNMMI Physics, 2021, 8, 79.	2.7	3
16	Clinical implication of 18F-NaF PET/computed tomography indexes of aortic calcification in coronary artery disease patients: correlations with cardiovascular risk factors. Nuclear Medicine Communications, 2020, 41, 58-64.	1.1	3
17	Initial M Staging of Rectal Cancer: FDG PET/MRI with a Hepatocyte-specific Contrast Agent versus Contrast-enhanced CT. Radiology, 2020, 294, 310-319.	7.3	31
18	Differential Expression of Glucose Transporters and Hexokinases in Prostate Cancer with a Neuroendocrine Gene Signature: A Mechanistic Perspective for <sup>18</sup> F-FDG Imaging of PSMA-Suppressed Tumors. Journal of Nuclear Medicine, 2020, 61, 904-910.	5.0	52

#	Article	IF	CITATIONS
19	Therapeutic efficacy of modified anti-miR21 in metastatic prostate cancer. Biochemical and Biophysical Research Communications, 2020, 529, 707-713.	2.1	11
20	Relationship of EGFR Mutation to Glucose Metabolic Activity and Asphericity of Metabolic Tumor Volume in Lung Adenocarcinoma. Nuclear Medicine and Molecular Imaging, 2020, 54, 175-182.	1.0	9
21	Reciprocal change in Glucose metabolism of Cancer and Immune Cells mediated by different Glucose Transporters predicts Immunotherapy response. Theranostics, 2020, 10, 9579-9590.	10.0	25
22	Efficacy and Safety of Human Serum Albumin–Cisplatin Complex in U87MG Xenograft Mouse Models. International Journal of Molecular Sciences, 2020, 21, 7932.	4.1	14
23	Tumor immune profiles noninvasively estimated by FDG PET with deep learning correlate with immunotherapy response in lung adenocarcinoma. Theranostics, 2020, 10, 10838-10848.	10.0	39
24	[18F]CB251 PET/MR imaging probe targeting translocator protein (TSPO) independent of its Polymorphism in a Neuroinflammation Model. Theranostics, 2020, 10, 9315-9331.	10.0	15
25	Spatial Normalization Using Early-Phase [18F]FP-CIT PET for Quantification of Striatal Dopamine Transporter Binding. Nuclear Medicine and Molecular Imaging, 2020, 54, 305-314.	1.0	4
26	Synthesis and Evaluation of 99mTc-Tricabonyl Labeled Isonitrile Conjugates for Prostate-Specific Membrane Antigen (PSMA) Image. Inorganics, 2020, 8, 5.	2.7	7
27	Predicting outcome of repair of medial meniscus posterior root tear with early osteoarthritis using bone single-photon emission computed tomography/computed tomography. Medicine (United States), 2020, 99, e21047.	1.0	2
28	Risk stratification of symptomatic brain metastases by clinical and FDG PET parameters for selective use of prophylactic cranial irradiation in patients with extensive disease of small cell lung cancer. Radiotherapy and Oncology, 2020, 143, 81-87.	0.6	9
29	A pan-cancer analysis of the clinical and genetic portraits of somatostatin receptor expressing tumor as a potential target of peptide receptor imaging and therapy. EJNMMI Research, 2020, 10, 42.	2.5	11
30	Conjugation of arginylglycylaspartic acid to human serum albumin decreases the tumor-targeting effect of albumin by hindering its secreted protein acidic and rich in cysteine-mediated accumulation in tumors. American Journal of Translational Research (discontinued), 2020, 12, 2488-2498.	0.0	1
31	Compartmental-modelling-based measurement of murine glomerular filtration rate using 18F-fluoride PET/CT. Scientific Reports, 2019, 9, 11269.	3.3	3
32	Versatile and Finely Tuned Albumin Nanoplatform based on Click Chemistry. Theranostics, 2019, 9, 3398-3409.	10.0	21
33	FDG PET/CT for the early prediction of RAI therapy response in patients with metastatic differentiated thyroid carcinoma. PLoS ONE, 2019, 14, e0218416.	2.5	18
34	Secreted protein acidic and rich in cysteine mediates active targeting of human serum albumin in U87MG xenograft mouse models. Theranostics, 2019, 9, 7447-7457.	10.0	45
35	Amyloid PET Quantification Via End-to-End Training of a Deep Learning. Nuclear Medicine and Molecular Imaging, 2019, 53, 340-348.	1.0	22
36	Multi-atlas cardiac PET segmentation. Physica Medica, 2019, 58, 32-39.	0.7	9

#	Article	IF	CITATIONS
37	Composite criteria using clinical and FDG PET/CT factors for predicting recurrence of hepatocellular carcinoma after living donor liver transplantation. European Radiology, 2019, 29, 6009-6017.	4.5	18
38	FDG PET for Evaluation of Bone Marrow Status in T-Cell Lymphoma. Clinical Nuclear Medicine, 2019, 44, 4-10.	1.3	20
39	Use of Molecular Imaging in Clinical Drug Development: a Systematic Review. Nuclear Medicine and Molecular Imaging, 2019, 53, 208-215.	1.0	12
40	Development of 99mTc-Labeled Human Serum Albumin with Prolonged Circulation by Chelate-then-Click Approach: A Potential Blood Pool Imaging Agent. Molecular Pharmaceutics, 2019, 16, 1586-1595.	4.6	13
41	Prognostic value of metabolic tumour volume on baseline 18F-FDG PET/CT in addition to NCCN-IPI in patients with diffuse large B-cell lymphoma: further stratification of the group with a high-risk NCCN-IPI. European Journal of Nuclear Medicine and Molecular Imaging, 2019, 46, 1417-1427.	6.4	49
42	Expanding therapeutic utility of carfilzomib for breast cancer therapy by novel albumin-coated nanocrystal formulation. Journal of Controlled Release, 2019, 302, 148-159.	9.9	41
43	Glucose-6-phosphatase Expression–Mediated [18F]FDG Efflux in Murine Inflammation and Cancer Models. Molecular Imaging and Biology, 2019, 21, 917-925.	2.6	5
44	Diagnostic Reference Levels for Adult Nuclear Medicine Imaging Established from the National Survey in Korea. Nuclear Medicine and Molecular Imaging, 2019, 53, 64-70.	1.0	16
45	Comprehensive gene expression analysis for exploring the association between glucose metabolism and differentiation of thyroid cancer. BMC Cancer, 2019, 19, 1260.	2.6	24
46	Trastuzumab Specific Epitope Evaluation as a Predictive and Prognostic Biomarker in Gastric Cancer Patients. Biomolecules, 2019, 9, 782.	4.0	7
47	Adenine Nucleotide Translocase 2 as an Enzyme Related to [18F] FDG Accumulation in Various Cancers. Molecular Imaging and Biology, 2019, 21, 722-730.	2.6	8
48	Neuroendocrine differentiation of prostate cancer leads to PSMA suppression. Endocrine-Related Cancer, 2019, 26, 131-146.	3.1	98
49	Dual-time point 18F-FDG PET/CT for the staging of oesophageal cancer: the best diagnostic performance by retention index for N-staging in non-calcified lymph nodes. European Journal of Nuclear Medicine and Molecular Imaging, 2018, 45, 1317-1328.	6.4	12
50	Whole-Body Voxel-Based Personalized Dosimetry: The Multiple Voxel S-Value Approach for Heterogeneous Media with Nonuniform Activity Distributions. Journal of Nuclear Medicine, 2018, 59, 1133-1139.	5.0	40
51	Giant Magnetic Heat Induction of Magnesiumâ€Ðoped γâ€Fe <sub>2</sub> O <sub>3</sub> Superparamagnetic Nanoparticles for Completely Killing Tumors. Advanced Materials, 2018, 30, 1704362.	21.0	99
52	<sup>18</sup> F-FEDAC as a Targeting Agent for Activated Macrophages in DBA/1 Mice with Collagen-Induced Arthritis: Comparison with <sup>18</sup> F-FDG. Journal of Nuclear Medicine, 2018, 59, 839-845.	5.0	23
53	Relation of EGFR Mutation Status to Metabolic Activity in Localized Lung Adenocarcinoma and Its Influence on the Use of FDG PET/CT Parameters in Prognosis. American Journal of Roentgenology, 2018, 210, 1346-1351.	2.2	16
54	The association between somatic and psychological discomfort and health-related quality of life according to the elderly and non-elderly. Quality of Life Research, 2018, 27, 673-681.	3.1	11

#	Article	IF	CITATIONS
55	Correlation of FDG PET/CT Findings with Long-Term Growth and Clinical Course of Abdominal Aortic Aneurysm. Nuclear Medicine and Molecular Imaging, 2018, 52, 46-52.	1.0	10
56	InÂvivo imaging of activated macrophages by 18F-FEDAC, a TSPO targeting PET ligand, in the use of biologic disease-modifying anti-rheumatic drugs (bDMARDs). Biochemical and Biophysical Research Communications, 2018, 506, 216-222.	2.1	12
57	Application of Quantitative Indexes of FDG PET to Treatment Response Evaluation in Indolent Lymphoma. Nuclear Medicine and Molecular Imaging, 2018, 52, 342-349.	1.0	12
58	Organic Nanomaterials: Liposomes, Albumin, Dendrimer, Polymeric Nanoparticles. Biological and Medical Physics Series, 2018, , 105-123.	0.4	5
59	Measurement of 68Ga-DOTATOC Uptake in the Thoracic Aorta and Its Correlation with Cardiovascular Risk. Nuclear Medicine and Molecular Imaging, 2018, 52, 279-286.	1.0	17
60	Prognostic value of simultaneous 18F-FDG PET/MRI using a combination of metabolo-volumetric parameters and apparent diffusion coefficient in treated head and neck cancer. EJNMMI Research, 2018, 8, 2.	2.5	21
61	Recurrence of Melanoma After Initial Treatment: Diagnostic Performance of FDG PET in Posttreatment Surveillance. Nuclear Medicine and Molecular Imaging, 2018, 52, 327-333.	1.0	9
62	Perceived needs for the information communication technology (ICT)â€based personalized health management program, and its association with information provision, healthâ€related quality of life (HRQOL), and decisional conflict in cancer patients. Psycho-Oncology, 2017, 26, 1810-1817.	2.3	9
63	Comparative evaluation of the algorithms for parametric mapping of the novel myocardial PET imaging agent 18F-FPTP. Annals of Nuclear Medicine, 2017, 31, 469-479.	2.2	3
64	Prediction of breast cancer recurrence using lymph node metabolic and volumetric parameters from 18F-FDG PET/CT in operable triple-negative breast cancer. European Journal of Nuclear Medicine and Molecular Imaging, 2017, 44, 1787-1795.	6.4	13
65	Neuronal nitric oxide synthase modulation of intracellular Ca2+ handling overrides fatty acid potentiation of cardiac inotropy in hypertensive rats. Pflugers Archiv European Journal of Physiology, 2017, 469, 1359-1371.	2.8	5
66	Discrepancy Between Tumor Antigen Distribution and Radiolabeled Antibody Binding in a Nude Mouse Xenograft Model of Human Melanoma. Cancer Biotherapy and Radiopharmaceuticals, 2017, 32, 83-89.	1.0	0
67	Superior Treatment Response and In-field Tumor Control in Epidermal Growth Factor Receptor-mutant Genotype of Stage III Nonsquamous Non–Small cell Lung Cancer Undergoing Definitive Concurrent Chemoradiotherapy. Clinical Lung Cancer, 2017, 18, e169-e178.	2.6	20
68	Comparative characteristics of quantitative indexes for 18F-FDG uptake and metabolic volume in sequentially obtained PET/MRI and PET/CT. Nuclear Medicine Communications, 2017, 38, 333-339.	1.1	1
69	Heterogeneity index evaluated by slope of linear regression on 18F-FDG PET/CT as a prognostic marker for predicting tumor recurrence in pancreatic ductal adenocarcinoma. European Journal of Nuclear Medicine and Molecular Imaging, 2017, 44, 1995-2003.	6.4	30
70	Simultaneous Detection of EGFR and VEGF in Colorectal Cancer using Fluorescence-Raman Endoscopy. Scientific Reports, 2017, 7, 1035.	3.3	33
71	Image-Based Analysis of Tumor Localization After Intra-Arterial Delivery of Technetium-99m-Labeled SPIO Using SPECT/CT and MRI. Molecular Imaging, 2017, 16, 153601211668900.	1.4	9
72	Influence of Androgen Deprivation Therapy on the Uptake of PSMA-Targeted Agents: Emerging Opportunities and Challenges. Nuclear Medicine and Molecular Imaging, 2017, 51, 202-211.	1.0	45

5

#	Article	IF	CITATIONS
73	Clinical Significance of Pretreatment FDG PET/CT in MIBG-Avid Pediatric Neuroblastoma. Nuclear Medicine and Molecular Imaging, 2017, 51, 154-160.	1.0	11
74	Comparison of Quantitative Methods on FDG PET/CT for Treatment Response Evaluation of Metastatic Colorectal Cancer. Nuclear Medicine and Molecular Imaging, 2017, 51, 147-153.	1.0	11
75	Feasibility of sentinel lymph node dissection using Tc-99m phytate in papillary thyroid carcinoma. Annals of Surgical Treatment and Research, 2017, 93, 240.	1.0	10
76	Thyroid-Related Protein Expression in the Human Thymus. International Journal of Endocrinology, 2017, 2017, 1-10.	1.5	7
77	Visualization of exosome-mediated miR-210 transfer from hypoxic tumor cells. Oncotarget, 2017, 8, 9899-9910.	1.8	115
78	The Potential Roles of Radionanomedicine and Radioexosomics in Prostate Cancer Research and Treatment. Current Pharmaceutical Design, 2017, 23, 2976-2990.	1.9	3
79	PET and Other Functional Imaging. , 2017, , 123-129.		0
80	Abstract 3733: Adenine nucleotide translocase2 mediates18F-FDG uptake in dedifferentiated thyroid cancer. , 2017, , .		0
81	Abstract 2864: Tumor targeting and imaging using64Cu labeled cyclic RGD conjugated human serum albumin via click chemistry. , 2017, , .		0
82	Dihydropyrimidine Dehydrogenase Is a Prognostic Marker for Mesenchymal Stem Cell-Mediated Cytosine Deaminase Gene and 5-Fluorocytosine Prodrug Therapy for the Treatment of Recurrent Gliomas. Theranostics, 2016, 6, 1477-1490.	10.0	27
83	Radiation Dose from Whole-Body F-18 Fluorodeoxyglucose Positron Emission Tomography/Computed Tomography: Nationwide Survey in Korea. Journal of Korean Medical Science, 2016, 31, S69.	2.5	37
84	History and Organizations for Radiological Protection. Journal of Korean Medical Science, 2016, 31, S4.	2.5	6
85	Prognostic Implications of the SUVmax of Primary Tumors and Metastatic Lymph Node Measured by 18F-FDG PET in Patients With Uterine Cervical Cancer. Clinical Nuclear Medicine, 2016, 41, 34-40.	1.3	52
86	Diagnostic performance of 18F-FDG-labeled white blood cell PET/CT for cyst infection in patients with autosomal dominant polycystic kidney disease. Nuclear Medicine Communications, 2016, 37, 493-498.	1.1	16
87	Prospective investigation and literature review of tolerance dose on salivary glands using quantitative salivary gland scintigraphy in the intensityâ€modulated radiotherapy era. Head and Neck, 2016, 38, E1746-55.	2.0	13
88	Gray matter correlates of dopaminergic degeneration in <scp>P</scp> arkinson's disease: A hybrid <scp>PET/MR</scp> study using <sup>18</sup> <scp>F</scp> â€ <scp>FP</scp> â€ <scp>CIT</scp> . Human Brain Mapping, 2016, 37, 1710-1721.	3.6	27
89	Prognostic Value of Metabolic and Volumetric Parameters of Preoperative FDG-PET/CT in Patients With Resectable Pancreatic Cancer. Medicine (United States), 2016, 95, e3686.	1.0	32
90	Preclinical evaluation of isostructural Tc-99m- and Re-188-folate-Gly-Gly-Cys-Glu for folate receptor-positive tumor targeting. Annals of Nuclear Medicine, 2016, 30, 369-379.	2.2	10

#	Article	IF	CITATIONS
91	Colorectal Cancer Liver Metastases: Diagnostic Performance and Prognostic Value of PET/MR Imaging. Radiology, 2016, 280, 782-792.	7.3	58
92	Development of Drugs and Technology for Radiation Theragnosis. Nuclear Engineering and Technology, 2016, 48, 597-607.	2.3	7
93	Plasmablastic lymphoma exclusively involving bones mimicking osteosarcoma in an immunocompetent patient. Medicine (United States), 2016, 95, e4241.	1.0	5
94	Phase analysis of gated myocardial perfusion single-photon emission computed tomography after coronary artery bypass graft surgery. Nuclear Medicine Communications, 2016, 37, 1139-1147.	1.1	7
95	Prognostic Value of 68Ga-NOTA-RGD PET/CT for Predicting Disease-Free Survival for Patients With Breast Cancer Undergoing Neoadjuvant Chemotherapy and Surgery. Clinical Nuclear Medicine, 2016, 41, 614-620.	1.3	10
96	Appropriate margin thresholds for isocontour metabolic volumetry of fluorine-18 fluorodeoxyglucose PET in sarcoma. Nuclear Medicine Communications, 2016, 37, 1088-1094.	1.1	10
97	A new fluorescence/PET probe for targeting intracellular human telomerase reverse transcriptase (hTERT) using Tat peptide-conjugated IgM. Biochemical and Biophysical Research Communications, 2016, 477, 483-489.	2.1	12
98	Feasibility of simultaneous 18F-FDG PET/MRI for the quantitative volumetric and metabolic measurements of abdominal fat tissues using fat segmentation. Nuclear Medicine Communications, 2016, 37, 616-622.	1.1	7
99	GPR119: a promising target for nonalcoholic fatty liver disease. FASEB Journal, 2016, 30, 324-335.	0.5	38
100	Early prediction of response to neoadjuvant chemotherapy in breast cancer patients: comparison of single-voxel 1H-magnetic resonance spectroscopy and 18F-fluorodeoxyglucose positron emission tomography. European Radiology, 2016, 26, 2279-2290.	4.5	14
101	Prediction of Posttransplantation Recurrence of Hepatocellular Carcinoma Using Metabolic and Volumetric Indices of <sup>18</sup> F-FDG PET/CT. Journal of Nuclear Medicine, 2016, 57, 1045-1051.	5.0	37
102	Atlas and Anatomy of PET/CT. , 2016, , 199-442.		0
103	Total Lesion Clycolysis in Positron Emission Tomography Can Predict Gefitinib Outcomes in Non–Small-Cell Lung Cancer with Activating EGFR Mutation. Journal of Thoracic Oncology, 2015, 10, 1189-1194.	1.1	26
104	Relationship between Apoptosis Imaging and Radioiodine Therapy in Tumor Cells with Different Sodium Iodide Symporter Gene Expression. Molecular Imaging, 2015, 14, 7290.2014.00050.	1.4	6
105	The risk of second primary malignancy is increased in differentiated thyroid cancer patients with a cumulative <sup>131</sup> I dose over 37 <scp>GB</scp> q. Clinical Endocrinology, 2015, 83, 117-123.	2.4	29
106	PET/CT-Based Dosimetry in 90Y-Microsphere Selective Internal Radiation Therapy. Medicine (United) Tj ETQq0 0 (	0 rgBT /Ov	erlock 10 Tf
107	Clinical Performance of Whole-Body 18F-FDG PET/Dixon-VIBE, T1-Weighted, and T2-Weighted MRI Protocol in Colorectal Cancer. Clinical Nuclear Medicine, 2015, 40, e392-e398.	1.3	17

108 Hemodynamic Significance of Internal Carotid or Middle Cerebral Artery Stenosis Detected on Magnetic Resonance Angiography. Yonsei Medical Journal, 2015, 56, 1686.

2.2 5

#	Article	IF	CITATIONS
109	Codon-optimized Human Sodium Iodide Symporter (opt-hNIS) as a Sensitive Reporter and Efficient Therapeutic Gene. Theranostics, 2015, 5, 86-96.	10.0	21
110	Glycosylation of Sodium/Iodide Symporter (NIS) Regulates Its Membrane Translocation and Radioiodine Uptake. PLoS ONE, 2015, 10, e0142984.	2.5	30
111	Correlation between 18F-FDG uptake on PET/CT and prognostic factors in triple-negative breast cancer. European Radiology, 2015, 25, 3314-3321.	4.5	34
112	Prognostic Value of Metabolic Tumor Volume on 11C-Methionine PET in Predicting Progression-Free Survival in High-Grade Glioma. Nuclear Medicine and Molecular Imaging, 2015, 49, 291-297.	1.0	34
113	Serum thyroglobulin level after radioiodine therapy (Day 3) to predict successful ablation of thyroid remnant in postoperative thyroid cancer. Annals of Nuclear Medicine, 2015, 29, 184-189.	2.2	15
114	Orotic Acid Induces Hypertension Associated with Impaired Endothelial Nitric Oxide Synthesis. Toxicological Sciences, 2015, 144, 307-317.	3.1	13
115	Update on nodal staging in non-small cell lung cancer with integrated positron emission tomography/computed tomography: a meta-analysis. Annals of Nuclear Medicine, 2015, 29, 409-419.	2.2	60
116	Usefulness of MRI-assisted metabolic volumetric parameters provided by simultaneous 18F-fluorocholine PET/MRI for primary prostate cancer characterization. European Journal of Nuclear Medicine and Molecular Imaging, 2015, 42, 1247-1256.	6.4	32
117	Usefulness of 131I-SPECT/CT and 18F-FDG PET/CT in Evaluating Successful 131I and Retinoic Acid Combined Therapy in a Patient with Metastatic Struma Ovarii. Nuclear Medicine and Molecular Imaging, 2015, 49, 52-56.	1.0	7
118	Radionuclide-labeled nanostructures for In Vivo imaging of cancer. Nano Convergence, 2015, 2, .	12.1	13
119	Prognostic Value of SUVmean in Oropharyngeal and Hypopharyngeal Cancers. Clinical Nuclear Medicine, 2015, 40, 9-13.	1.3	18
120	18F-Fluorodeoxyglucose and 11C-methionine positron emission tomography in relation to methyl-guanine methyltransferase promoter methylation in high-grade gliomas. Nuclear Medicine Communications, 2015, 36, 211-218.	1.1	11
121	Fluorescence-Raman Dual Modal Endoscopic System for Multiplexed Molecular Diagnostics. Scientific Reports, 2015, 5, 9455.	3.3	73
122	Association between information provision and decisional conflict in cancer patients. Annals of Oncology, 2015, 26, 1974-1980.	1.2	21
123	Comparison of Diagnostic Sensitivity and Quantitative Indices Between 68Ga-DOTATOC PET/CT and 1111n-Pentetreotide SPECT/CT in Neuroendocrine Tumors: a Preliminary Report. Nuclear Medicine and Molecular Imaging, 2015, 49, 284-290.	1.0	29
124	Evaluation of the novel near-infrared fluorescence tracers pullulan polymer nanogel and indocyanine green/γ-glutamic acid complex for sentinel lymph node navigation surgery in large animal models. Gastric Cancer, 2015, 18, 55-64.	5.3	50
125	Diagnostic values of thyroglobulin measurement in fine-needle aspiration of lymph nodes in patients with thyroid cancer. Endocrine, 2015, 49, 70-77.	2.3	38
126	Prognostic value of volumetric parameters of 18F-FDG PET in non-small-cell lung cancer: a meta-analysis. European Journal of Nuclear Medicine and Molecular Imaging, 2015, 42, 241-251.	6.4	203

#	Article	IF	CITATIONS
127	Comparison of SPECT/CT and MRI in Diagnosing Symptomatic Lesions in Ankle and Foot Pain Patients: Diagnostic Performance and Relation to Lesion Type. PLoS ONE, 2015, 10, e0117583.	2.5	46
128	A novel hNIS/tdTomato fusion reporter for visualizing the relationship between the cellular localization of sodium iodide symporter and its iodine uptake function under heat shock treatment. Molecular Imaging, 2015, 14, .	1.4	1
129	The Value of SPECT/CT in Localizing Pain Site and Prediction of Treatment Response in Patients with Chronic Low Back Pain. Journal of Korean Medical Science, 2014, 29, 1711.	2.5	21
130	Does 18F-FDG Positron Emission Tomography-Computed Tomography Have a Role in Initial Staging of Hepatocellular Carcinoma?. PLoS ONE, 2014, 9, e105679.	2.5	43
131	The Effectiveness of Recombinant Human Thyroid-Stimulating Hormone versus Thyroid Hormone Withdrawal Prior to Radioiodine Remnant Ablation in Thyroid Cancer: A Meta-Analysis of Randomized Controlled Trials. Journal of Korean Medical Science, 2014, 29, 811.	2.5	14
132	Monitoring differentiated thyroid cancer patients with negative serum thyroglobulin. Nuklearmedizin - NuclearMedicine, 2014, 53, 32-38.	0.7	6
133	Prognostic Value of Metabolic Tumor Volume and Total Lesion Glycolysis in Head and Neck Cancer: A Systematic Review and Meta-Analysis. Journal of Nuclear Medicine, 2014, 55, 884-890.	5.0	257
134	Functional evaluation of parathyroid adenoma using 99mTc-MIBI parathyroid SPECT/CT. Nuclear Medicine Communications, 2014, 35, 649-654.	1.1	26
135	Correlation of 11C-methionine PET and diffusion-weighted MRI. Nuclear Medicine Communications, 2014, 35, 720-726.	1.1	14
136	Total lesion glycolysis as the best 18F-FDG PET/CT parameter in differentiating intermediate–high risk adrenal incidentaloma. Nuclear Medicine Communications, 2014, 35, 606-612.	1.1	10
137	Incidental thyroid cancer detected by 18F-FDG PET. Nuclear Medicine Communications, 2014, 35, 453-458.	1.1	5
138	Segmentation-Based MR Attenuation Correction Including Bones Also Affects Quantitation in Brain Studies: An Initial Result of <sup>18</sup> F-FP-CIT PET/MR for Patients with Parkinsonism. Journal of Nuclear Medicine, 2014, 55, 1617-1622.	5.0	24
139	Evaluation of Azygous Vein Aneurysm Using Integrated PET/MRI. Nuclear Medicine and Molecular Imaging, 2014, 48, 161-162.	1.0	3
140	Usefulness of Integrated PET/MRI in Head and Neck Cancer: A Preliminary Study. Nuclear Medicine and Molecular Imaging, 2014, 48, 98-105.	1.0	34
141	Recent Trends in PET Image Interpretations Using Volumetric and Texture-based Quantification Methods in Nuclear Oncology. Nuclear Medicine and Molecular Imaging, 2014, 48, 1-15.	1.0	86
142	18F-FDG uptake in breast cancer correlates with immunohistochemically defined subtypes. European Radiology, 2014, 24, 610-618.	4.5	81
143	In Vivo Evaluation of Angiogenic Activity and Its Correlation with Efficacy of Indirect Revascularization Surgery in Pediatric Moyamoya Disease. Journal of Nuclear Medicine, 2014, 55, 1467-1472.	5.0	18
144	Preoperative PET/CT FDG standardized uptake value of pelvic lymph nodes as a significant prognostic factor in patients with uterine cervical cancer. European Journal of Nuclear Medicine and Molecular Imaging, 2014, 41, 674-681.	6.4	23

#	Article	lF	CITATIONS
145	Correlation of breast cancer subtypes, based on estrogen receptor, progesterone receptor, and HER2, with functional imaging parameters from 68Ga-RGD PET/CT and 18F-FDG PET/CT. European Journal of Nuclear Medicine and Molecular Imaging, 2014, 41, 1534-1543.	6.4	65
146	Autoclustering of Non-small Cell Lung Carcinoma Subtypes on 18F-FDG PET Using Texture Analysis: A Preliminary Result. Nuclear Medicine and Molecular Imaging, 2014, 48, 278-286.	1.0	60
147	In Vivo Bioluminescence Imaging of Transplanted Mesenchymal Stem Cells as a Potential Source for Pancreatic Regeneration. Molecular Imaging, 2014, 13, 7290.2014.00023.	1.4	4
148	Parametric Cerebrovascular Reserve Images Using Acetazolamide 99mTc-HMPAO SPECT: A Feasibility Study of Quantitative Assessment. Nuclear Medicine and Molecular Imaging, 2013, 47, 188-195.	1.0	5
149	Detection and Characterization of Parathyroid Adenoma/Hyperplasia for Preoperative Localization: Comparison Between 11C-Methionine PET/CT and 99mTc-Sestamibi Scintigraphy. Nuclear Medicine and Molecular Imaging, 2013, 47, 166-172.	1.0	24
150	Differential Diagnosis of Borderline Ovarian Tumors from Stage I Malignant Ovarian Tumors using FDG PET/CT. Nuclear Medicine and Molecular Imaging, 2013, 47, 81-88.	1.0	22
151	Predictive value of FDG PET/CT for pathologic axillary node involvement after neoadjuvant chemotherapy. Breast Cancer, 2013, 20, 167-173.	2.9	17
152	Background 18F-FDG uptake in positron emission mammography (PEM): Correlation with mammographic density and background parenchymal enhancement in breast MRI. European Journal of Radiology, 2013, 82, 1738-1742.	2.6	24
153	Heterogeneity Analysis of 18F-FDG Uptake in Differentiating Between Metastatic and Inflammatory Lymph Nodes in Adenocarcinoma of the Lung: Comparison with Other Parameters and its Application in a Clinical Setting. Nuclear Medicine and Molecular Imaging, 2013, 47, 232-241.	1.0	28
154	Metabolic and metastatic characteristics of ALK-rearranged lung adenocarcinoma on FDG PET/CT. Lung Cancer, 2013, 79, 242-247.	2.0	62
155	One-step detection of circulating tumor cells in ovarian cancer using enhanced fluorescent silica nanoparticles. International Journal of Nanomedicine, 2013, 8, 2247.	6.7	25
156	18F-FDG PET/CT features of pulmonary sclerosing hemangioma. Acta Radiologica, 2013, 54, 24-29.	1.1	27
157	Angiogenesis imaging in myocardial infarction using 68Ga-NOTA-RGD PET. Coronary Artery Disease, 2013, 24, 303-311.	0.7	26
158	Metabolic Characteristics of Castleman Disease on 18F-FDG PET in Relation to Clinical Implication. Clinical Nuclear Medicine, 2013, 38, 339-342.	1.3	47
159	Is It Safe to Eat Fish?. Journal of Korean Medical Science, 2013, 28, 1701.	2.5	0
160	RAI Treatment of Distant Metastasis of Thyroid Cancer. Journal of Korean Thyroid Association, 2013, 6, 49.	0.2	1
161	Mammography and ultrasonography evaluation of unexpected focal 18F-FDG uptakes in breast on PET/CT. Acta Radiologica, 2012, 53, 249-254.	1.1	10
162	Whole-Body Distribution and Radiation Dosimetry of <sup>68</sup> Ga-NOTA-RGD, a Positron Emission Tomography Agent for Angiogenesis Imaging. Cancer Biotherapy and Radiopharmaceuticals, 2012, 27, 65-71.	1.0	52

#	Article	IF	CITATIONS
163	Validation of Simple Quantification Methods for 18F-FP-CIT PET Using Automatic Delineation of Volumes of Interest Based on Statistical Probabilistic Anatomical Mapping and Isocontour Margin Setting. Nuclear Medicine and Molecular Imaging, 2012, 46, 254-260.	1.0	12
164	Physical limits of pure superparamagnetic Fe3O4 nanoparticles for a local hyperthermia agent in nanomedicine. Applied Physics Letters, 2012, 100, .	3.3	71
165	The hepatoprotective effects of adenine nucleotide translocator-2 against aging and oxidative stress. Free Radical Research, 2012, 46, 21-29.	3.3	12
166	Near-Infrared Emitting Polymer Nanogels for Efficient Sentinel Lymph Node Mapping. ACS Nano, 2012, 6, 7820-7831.	14.6	84
167	<i>In vivo</i> Molecular Imaging. , 2012, , 381-393.		0
168	Near infrared dye indocyanine green doped silica nanoparticles for biological imaging. Talanta, 2012, 99, 387-393.	5.5	58
169	Predictive role of post-treatment [18F]FDG PET/CT in patients with uterine cervical cancer. European Journal of Radiology, 2012, 81, e817-e822.	2.6	26
170	Development and <i>in vivo</i> imaging of a PET/MRI nanoprobe with enhanced NIR fluorescence by dye encapsulation. Nanomedicine, 2012, 7, 219-229.	3.3	53
171	Ischemia-Reperfusion Injury Leads to Distinct Temporal Cardiac Remodeling in Normal versus Diabetic Mice. PLoS ONE, 2012, 7, e30450.	2.5	33
172	Preoperative [ <sup>18</sup> F]FDG PET/CT predicts recurrence in patients with epithelial ovarian cancer. Journal of Gynecologic Oncology, 2012, 23, 28.	2.2	32
173	Ultrasensitive, Biocompatible, Quantumâ€Dotâ€Embedded Silica Nanoparticles for Bioimaging. Advanced Functional Materials, 2012, 22, 1843-1849.	14.9	123
174	A Case of Enterocutaneous Fistula Diagnosed with Tc-99m DTPA Fistulography Using Hybrid SPECT/CT. Nuclear Medicine and Molecular Imaging, 2012, 46, 111-114.	1.0	1
175	Comparison of diffusion-weighted MR imaging and FDG PET/CT to predict pathological complete response to neoadjuvant chemotherapy in patients with breast cancer. European Radiology, 2012, 22, 18-25.	4.5	91
176	Imaging sensitivity of dedicated positron emission mammography in relation to tumor size. Breast, 2012, 21, 66-71.	2.2	72
177	Prognostic Value of Preoperative Metabolic Tumor Volume and Total Lesion Glycolysis in Patients with Epithelial Ovarian Cancer. Annals of Surgical Oncology, 2012, 19, 1966-1972.	1.5	134
178	Imaging and quantification of metastatic melanoma cells in lymph nodes with a ferritin MR reporter in living mice. NMR in Biomedicine, 2012, 25, 737-745.	2.8	31
179	Selection and Characterization of Tenascin C Targeting Peptide. Molecules and Cells, 2012, 33, 71-78.	2.6	50
180	Heterodimerization of Glycosylated Insulin-Like Growth Factor-1 Receptors and Insulin Receptors in Cancer Cells Sensitive to Anti-IGF1R Antibody. PLoS ONE, 2012, 7, e33322.	2.5	41

#	Article	IF	CITATIONS
181	Prognostic value of metabolic tumor volume measured by FDG-PET/CT in patients with cervical cancer. Gynecologic Oncology, 2011, 120, 270-274.	1.4	121
182	Prognostic value of metabolic tumor volume measured by FDC-PET/CT in patients with cervical cancer. Gynecologic Oncology, 2011, 120, S113.	1.4	0
183	Positron Emission Tomography-Computed Tomography for Postoperative Surveillance in Non-Small Cell Lung Cancer. Annals of Thoracic Surgery, 2011, 92, 1826-1832.	1.3	58
184	Post-treatment [18F]FDG maximum standardized uptake value as a prognostic marker of recurrence in endometrial carcinoma. European Journal of Nuclear Medicine and Molecular Imaging, 2011, 38, 74-80.	6.4	14
185	Quantitative Measurement of Serum Hepatitis B Surface Antigen Using an Immunoradiometric Assay in Chronic Hepatitis B. Nuclear Medicine and Molecular Imaging, 2011, 45, 15-20.	1.0	3
186	Intratumoral Heterogeneous F-18 Fluorodeoxyglucose Uptake Corresponds with Glucose Transporter-1 and Ki-67 Expression in a Case of Krukenberg Tumor: Localization of Intratumoral Hypermetabolic Focus by Fused PET/MR Image. Nuclear Medicine and Molecular Imaging, 2011, 45, 139-144.	1.0	2
187	Nonfunctioning Periurethral Paraganglioma Incidentally Detected by FDG PET/CT. Nuclear Medicine and Molecular Imaging, 2011, 45, 145-148.	1.0	1
188	Diagnostic Performance of Three-Phase Bone Scan for Complex Regional Pain Syndrome Type 1 with Optimally Modified Image Criteria. Nuclear Medicine and Molecular Imaging, 2011, 45, 261-267.	1.0	22
189	Alternative Medical Treatment for Radioiodine-Refractory Thyroid Cancers. Nuclear Medicine and Molecular Imaging, 2011, 45, 241-247.	1.0	18
190	Early metabolic response using FDG PET/CT and molecular phenotypes of breast cancer treated with neoadjuvant chemotherapy. BMC Cancer, 2011, 11, 452.	2.6	61
191	Tumor Targeting and Imaging Using Cyclic RGDâ€PEGylated Gold Nanoparticle Probes with Directly Conjugated Iodineâ€125. Small, 2011, 7, 2052-2060.	10.0	173
192	The assessment of breast cancer response to neoadjuvant chemotherapy: comparison of magnetic resonance imaging and <sup>18</sup> F-fluorodeoxyglucose positron emission tomography. Acta Radiologica, 2011, 52, 21-28.	1.1	33
193	P2-09-13: The Value of FDG PET/CT in Screening Detected Breast Cancer Patients , 2011, , .		0
194	Radioiodine Treatment of Differentiated Thyroid Carcinoma: The Experience at Seoul National University Hospital. Current Medical Imaging, 2010, 6, 2-7.	0.8	2
195	Extravasation of Hydroxymethylene Diphosphonate–Induced Subcutaneous Inflammation, Histologically Demonstrated in BALB/c Mice: FIGURE 1 Journal of Nuclear Medicine, 2010, 51, 1573-1575.	5.0	4
196	Value of Combined Interpretation of Computed Tomography Response and Positron Emission Tomography Response for Prediction of Prognosis After Neoadjuvant Chemotherapy in Non-small Cell Lung Cancer. Journal of Thoracic Oncology, 2010, 5, 497-503.	1.1	33
197	Preoperative [18F]FDG PET/CT maximum standardized uptake value predicts recurrence of uterine cervical cancer. European Journal of Nuclear Medicine and Molecular Imaging, 2010, 37, 1467-1473.	6.4	49
198	Sodium Iodide Symporter and the Radioiodine Treatment of Thyroid Carcinoma. Nuclear Medicine and Molecular Imaging, 2010, 44, 4-14.	1.0	45

#	Article	IF	CITATIONS
199	Behavior and Awareness of Thyroid Cancer Patients in Korea Having Non-Hospitalized Low-Dose Radioiodine Treatment with Regard to Radiation Safety. Nuclear Medicine and Molecular Imaging, 2010, 44, 267-272.	1.0	2
200	In Vivo Imaging of Sentinel Nodes Using Fluorescent Silica Nanoparticles in Living Mice. Molecular Imaging and Biology, 2010, 12, 155-162.	2.6	30
201	Role of magnetic resonance imaging and positron emission tomography/computed tomography in preoperative lymph node detection of uterine cervical cancer. American Journal of Obstetrics and Gynecology, 2010, 203, 156.e1-156.e5.	1.3	45
202	The Role of Postoperative External Beam Radiotherapy in Differentiated Thyroid Cancer with Focal Anaplastic Change. International Journal of Radiation Oncology Biology Physics, 2010, 78, S432.	0.8	0
203	Differentiating radiation necrosis from tumor recurrence in high-grade gliomas: Assessing the efficacy of 18F-FDG PET, 11C-methionine PET and perfusion MRI. Clinical Neurology and Neurosurgery, 2010, 112, 758-765.	1.4	144
204	Angiogenesis Imaging Using 68Ga-RGD PET: Preliminary Report from Seoul National University Hospital. Current Medical Imaging, 2010, 6, 56-59.	0.8	1
205	Abstract P2-09-01: Serial [18F] FDG-PET after the 2nd Cycle of Preoperative Chemotherapy Is Predictive for Pathological Complete Response in Stage II/III Breast Cancer. , 2010, , .		0
206	Prediction of Tumor Recurrence by <sup>18</sup> F-FDG PET in Liver Transplantation for Hepatocellular Carcinoma. Journal of Nuclear Medicine, 2009, 50, 682-687.	5.0	154
207	Cancer screening using 18F-FDG PET/CT in Korean asymptomatic volunteers: a preliminary report. Annals of Nuclear Medicine, 2009, 23, 685-691.	2.2	41
208	18F-FDG PET in the assessment of tumor grade and prediction of tumor recurrence in intracranial meningioma. European Journal of Nuclear Medicine and Molecular Imaging, 2009, 36, 1574-1582.	6.4	76
209	Comparison of two full automatic synthesis methods of 9-(4-[18F]fluoro-3-hydroxymethylbutyl)guanine using different chemistry modules. Applied Radiation and Isotopes, 2009, 67, 1758-1763.	1.5	5
210	EGFR gene copy number in adenocarcinoma of the lung by FISH analysis: Investigation of significantly related factors on CT, FDG-PET, and histopathology. Lung Cancer, 2009, 64, 179-186.	2.0	31
211	Early Prediction of Response to First-Line Therapy Using Integrated 18F-FDG PET/CT for Patients with Advanced/Metastatic Non-small Cell Lung Cancer. Journal of Thoracic Oncology, 2009, 4, 816-821.	1.1	76
212	Upregulated HSP27 in human breast cancer cells reduces Herceptin susceptibility by increasing Her2 protein stability. BMC Cancer, 2008, 8, 286.	2.6	97
213	Preclinical Efficacy of the c-Met Inhibitor CE-355621 in a U87 MG Mouse Xenograft Model Evaluated by <sup>18</sup> F-FDG Small-Animal PET. Journal of Nuclear Medicine, 2008, 49, 129-134.	5.0	201
214	A Prospective Evaluation of <sup>18</sup> F-FDG and <sup>11</sup> C-Acetate PET/CT for Detection of Primary and Metastatic Hepatocellular Carcinoma. Journal of Nuclear Medicine, 2008, 49, 1912-1921.	5.0	242
215	breast cancer, advanced. Annals of Oncology, 2008, 19, viii63-viii76.	1.2	4
216	Sentinel node identification rate, but not accuracy, is significantly decreased after pre-operative chemotherapy in axillary node-positive breast cancer patients. Breast Cancer Research and Treatment, 2007, 102, 283-288.	2.5	87

#	Article	IF	CITATIONS
217	Assessment of lymph node metastases using 18F-FDG PET in patients with advanced gastric cancer. European Journal of Nuclear Medicine and Molecular Imaging, 2006, 33, 148-155.	6.4	168
218	Clinical impact of FDG-PET imaging in post-therapy surveillance of uterine cervical cancer: From diagnosis to prognosis. Gynecologic Oncology, 2006, 103, 165-170.	1.4	65
219	Comparison of the accuracy of magnetic resonance imaging and positron emission tomography/computed tomography in the presurgical detection of lymph node metastases in patients with uterine cervical carcinoma. Cancer, 2006, 106, 914-922.	4.1	310
220	Incidental ovarian 18F-FDG accumulation on PET: correlation with the menstrual cycle. European Journal of Nuclear Medicine and Molecular Imaging, 2005, 32, 757-763.	6.4	81
221	Comparison of [14C]FMAU, [3H]FEAU, [14C]FIAU, and [3H]PCV for Monitoring Reporter Gene Expression of Wild Type and Mutant Herpes Simplex Virus Type 1 Thymidine Kinase in Cell Culture. Molecular Imaging and Biology, 2005, 7, 296-303.	2.6	59
222	Simple Pulmonary Eosinophilia Evaluated by Means of FDG PET: the Findings of 14 Cases. Korean Journal of Radiology, 2005, 6, 208.	3.4	16
223	Development of Korean Standard Brain Templates. Journal of Korean Medical Science, 2005, 20, 483.	2.5	65
224	Role of positron emission tomography in pretreatment lymph node staging of uterine cervical cancer: A prospective surgicopathologic correlation study. European Journal of Cancer, 2005, 41, 2086-2092.	2.8	81
225	Intrathoracic Gastric Emptying of Solid Food After Esophagectomy for Esophageal Cancer. Annals of Thoracic Surgery, 2005, 80, 443-447.	1.3	66
226	Prevalence and Risk of Cancer of Focal Thyroid Incidentaloma Identified by18F-Fluorodeoxyglucose Positron Emission Tomography for Metastasis Evaluation and Cancer Screening in Healthy Subjects. Journal of Clinical Endocrinology and Metabolism, 2003, 88, 4100-4104.	3.6	264
227	Neoadjuvant Chemotherapy Decreases the Identification Rate of Sentinel Lymph Node Biopsy. Journal of Korean Breast Cancer Society, 2003, 6, 95.	0.1	2
228	Superiority of HMPAO Ictal SPECT to ECD Ictal SPECT in Localizing the Epileptogenic Zone. Epilepsia, 2002, 43, 263-269.	5.1	28
229	Partial Volume Correction of Simulated PET and 18F FDG PET from 14 Normal Brains. , 2002, , 153-157.		0
230	Quantification of F-18 FDG PET Images in Temporal Lobe Epilepsy Patients Using Probabilistic Brain Atlas. NeuroImage, 2001, 14, 1-6.	4.2	65
231	Disparity of Perfusion and Glucose Metabolism of Epileptogenic Zones in Temporal Lobe Epilepsy Demonstrated by SPM/SPAM Analysis on 15 O Water PET, [ 18 F]FDGâ€PET, and [ 99m Tc]â€HMPAO SPECT. Epilepsia, 2001, 42, 1515-1522.	5.1	48
232	Diagnostic Performance of [ 18 F]FDGâ€₽ET and Ictal [ 99m Tc]â€HMPAO SPECT in Occipital Lobe Epilepsy. Epilepsia, 2001, 42, 1531-1540.	5.1	51
233	Late postictal residual perfusion abnormality in epileptogenic zone found on 6-hour postictal SPECT. Neurology, 2000, 55, 835-841.	1.1	27
234	Reporter Gene Imaging with PET/SPECT. , 0, , 70-87.		2

Reporter Gene Imaging with PET/SPECT. , 0, , 70-87. 234

#	Article	IF	CITATIONS
235	Phase I Clinical Trial of Prostate-Specific Membrane Antigen-Targeting <sup>68</sup> Ga-NGUL PET/CT in Healthy Volunteers and Patients with Prostate Cancer. Korean Journal of Radiology, 0, 23, .	3.4	2